# Microporous Polymer Networks for Carbon Capture Applications

Beatriz Lopez-Iglesias[1], Fabián Suárez-García[2], Carla Aguilar-Lugo[3], Alfonso González Ortega[4], Camino Bartolomé[1], Jesús M. Martínez-Ilarduya[1], José G. de la Campa[3], Ángel E. Lozano[1,3,5*], Cristina Álvarez[3*]

1. IU CINQUIMA, Universidad de Valladolid, Paseo Belén 5, E-47011 Valladolid, Spain.

2. Instituto Nacional del Carbón, INCAR-CSIC, Dr. Ingeniero Francisco Pintado 26, E-33011 Oviedo, Spain.

3. Department of Applied Macromolecular Chemistry, Instituto de Ciencia y Tecnología de Polímeros, ICTP-CSIC, Juan de la Cierva 3, E-28006 Madrid, Spain.

4. Department of Organic Chemistry, Universidad de Valladolid, Facultad de Ciencias, Paseo Belén 7, E-47011 Valladolid, Spain.

5. SMAP, UA-UVA_CSIC, Associated Research Unit to CSIC. Universidad de Valladolid, Facultad de Ciencias, Paseo Belén 7, E-47011 Valladolid, Spain.

Table of Content
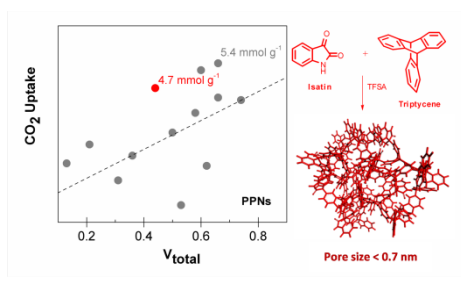
Abstract

A new generation of porous polymer networks, PPNs, has been obtained in quantitative yield by reacting in superacidic media two rigid trifunctional aromatic monomers (1,3,5-triphenylbenzene and triptycene) with two ketones having electron-withdrawing groups (trifluoroacetophenone and isatin). The resulting amorphous networks are microporous materials, with moderate BET surface areas (from 580 to 790 m^2 g^{-1}) and have high thermal stability. In particular, isatin yields networks with a very high narrow

microporosity contribution, 82% for triptycene and 64% for 1,3,5-triphenylbenzene. The existence of favorable interactions between lactams and CO_2 molecules has been stated. The materials show excellent CO_2 uptakes (up to 207 mg g^{-1} at 0 ℃/1 bar) and can be regenerated by vacuum, without heating. Under post-combustion conditions, their CO_2/N_2 selectivities are comparable to those of other organic porous networks. Because of the easily scalable synthetic method and their favorable characteristics, these materials are very promising as industrial adsorbents.

INTRODUCTION

The search of new materials able to revert in any form the global warming is mandatory for our civilization. Global warming is a serious risk for our society due to the expected calamitous effects in the environment and human health. Therefore, our society should, at least, maintain the CO_2 atmospheric value as low as possible.[1-6]

Over the last few years, novel solid adsorbent materials have been explored to be used in carbon capture and storage (CCS) technologies, which have the greatest likelihood of reducing CO_2 emissions to the atmosphere.[7,8] An efficient solid adsorbent material should be highly selective towards CO_2 over other gases present in the stream (notably N_2, H_2, CH_4 and H_2O), have a high CO_2 uptake capacity at low and high gas pressure, be physical and chemically stable under operational conditions, be easily regenerated with low energy input, maintain its performance under a humid atmosphere and repeated uses, and be prepared from low-cost raw materials.

In the search for efficient solid adsorbents for CO_2 capture, the amorphous porous materials have garnered much attention in recent years.[9-11] These materials are tailored using covalently linked molecular building blocks to possess high porosities and chemical and physical stabilities.[12] Moreover, these blocks are often derived from aromatic

monomers, either linked directly or by other rigid groups, to prevent the networks from collapsing. These networks have been prepared using a great diversity of chemistry and have been named in many different ways, such as hyper-cross-linking polymers (HCPs),[13-15] porous aromatic frameworks (PAFs),[16-19] porous polymer networks (PPNs),[20,21] polymeric organic frameworks (POFs),[22] porous benzimidazole-benzoxazole- benzothiazole- linked polymers (BILPs, BOLPs and BTLPs),[23-25] porous imine-linked polymers frameworks,[26] covalent triazine-based frameworks (CTFs),[27-29] or PIM-based networks.[30] However, in many cases, the monomers employed have to carry several functional groups (formed by multi-steps reactions), which increases notably their cost and limits their use for practical applications.

Recently, the Scholl reaction, which is able to form sp^2-sp^2 aromatic bonds by using Lewis acids, has been described for the preparation of PPNs.[31] This route is especially attractive because it allows access to polymer networks with high microporosity from available and inexpensive starting materials and reagents.[32,33]

Another promising reaction to prepare PPNs, which has never been used according to our knowledge, consists of the acid (Lewis or Brönsted) catalyzed condensation at low temperatures of ketones or aldehydes with aromatic compounds, which is described in the literature as the hydroxyalkylation reaction.[34]

It has been shown that acid-catalyzed condensation reaction of ketones with aromatic substrates initially produces tri-substituted alcohols, which undergo further protonation of the hydroxyl group and subsequent reaction with another molecule of arene to provide the corresponding tetra-substituted methane derivatives. However, the carbocationic nature of carboxonium ions is limited by strong electronic delocalization resulting from contributions of the oxonium forms. This restricts the reactions at the carbocationic center to those with efficient nucleophiles. Only a few microporous polymer networks of this

3

type have been obtained by employing common ketones, strong Brönsted acids, electron-rich aromatic moieties and high reaction temperatures.[35]

According to Olah's definition of superelectrophiles, under superacidic conditions, further protonation or protosolvation of the protonated aldehydes or ketones is possible, which leads to very reactive intermediates (superelectrophiles), that is, electrophiles of doubly electron-deficient (dipositive) nature whose reactivity significantly exceeds that of their parent monocations under conventional reaction conditions.[36-38] This super-electrophilic or multi-ionic intermediate can undergo successive condensation reactions with weaker nucleophiles, and thus it is possible the reaction even with deactivated aromatic rings (Scheme 1).
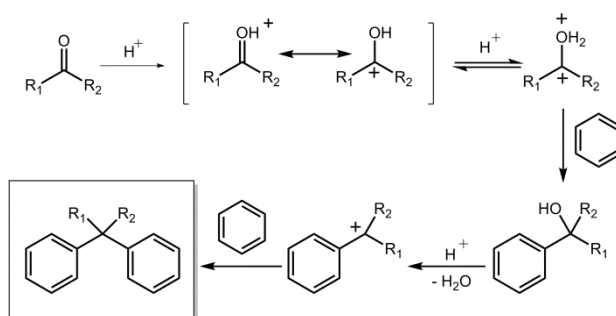

Scheme 1. Hydroxyalkylation reaction under superacidic conditions.

Irrespective of the mechanism, the reactivity of the protonated carbonyl group is further increased by the presence of electron-withdrawing groups (EWGs). For example, 1,2-dicarbonyl groups form highly reactive intermediates in superacidic conditions. Carbonyl compounds bearing other electron-withdrawing substituents have been also used for this chemistry. For example, superacid-catalyzed condensation reactions of trifluoromethyl ketones occur with somewhat deactivated aromatic hydrocarbons to give diaryl derivatives in excellent yields. This is a well-known case of monocationic electrophile

that reacts because the adjacent electron-withdrawing trifluoromethyl group enhances significantly the electrophylicity of the carbocation.[39]

Based on this high reactivity, Zolotukhin et al. have described the synthesis of high molecular weight, linear polymers, by reaction of activated ketones (2,2,2-trifluoroacetophenone, isatin, ninhydrin, etc.) with several aromatic compounds, (biphenyl, p-terphenyl, p-quaterphenyl, biphenol, binaphtol, etc.), using superacids (trifluoromethanesulfonic acid, methanesulfonic acid, trifluoroacetic acid and mixtures of them).[40-44] It has been feasible to obtain polymers with high viscosity and excellent mechanical properties, by far better than those attained by other polymerization techniques that led to the same macromolecular structures. Moreover, the thermal and chemical stability of these polymers resulted to be very high. When the monomers are well chosen, it is possible to make easy chemical modification on the polymers: nitration, sulfonation, etc., what could bring about materials with tailor-made properties and with better ability to interact with specific molecules.

Therefore, in the present work, we have considered the reaction of trifunctional aromatic molecules having a specific symmetry (triptycene; a 3D paddle wheel structure having a D_{3h} symmetry, and 1,3,5-triphenylbenzene, with a C_3 symmetry), with activated ketones (1H-indole-2,3-dione, named isatin, and 2,2,2-trifluoroacetophenone), which act as bifunctional monomers, to prepare crosslinked, rigid, amorphous, tridimensional networks, designed to yield nanoporous materials with high fractional free volume (Scheme 2). The proposed reaction is very easy to carry out with high conversion, and it is possible to scale-up this methodology to produce high amounts of materials. The influence of the monomeric structure on the porosity and surface area of the networks has been studied along with their ability to take a high amount of CO_2.
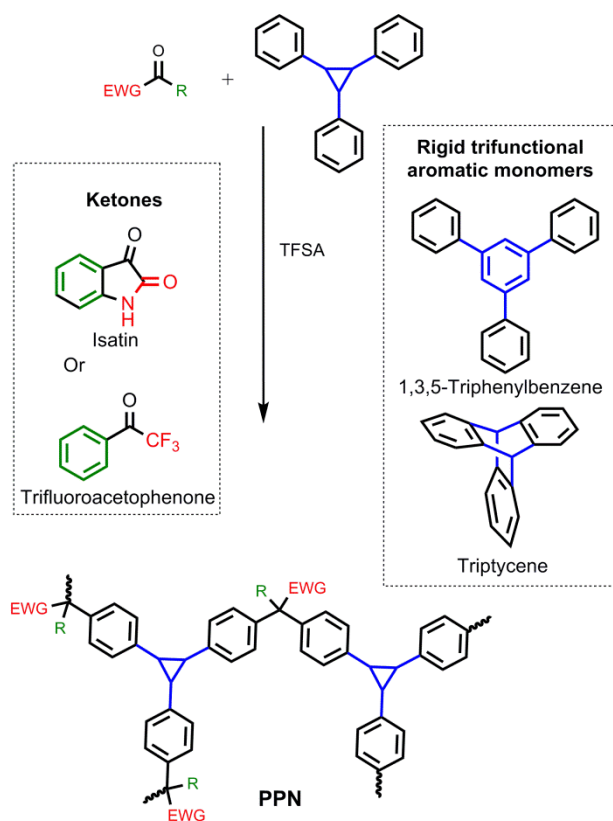
Scheme 2. Synthesis of tridimensional networks by reaction of a trifunctional arene with a difunctional carbonyl compound bearing electron-withdrawing groups (EWGs).

2. EXPERIMENTAL PART

2.1. Materials

Acetophenone (99%), silicon tetrachloride (99%), isatin (1H-indole-2,3-dione) (99%), 2,2,2-trifluoroacetophenone (TFAP, 99%), and anhydrous chloroform were purchased from Sigma-Aldrich. TFAP was previously distilled and stored in a Schlenk tube under nitrogen atmosphere. Isatin was dried at 60 °C for 2 h, under vacuum, before use. Trifluromethanesulfonic acid (TFSA) (99%) was supplied by Apollo Scientific, and triptycene (98%) was purchased from abcr GmbH.

Synthesis of 1,3,5-triphenylbenzene (1,3,5-TPB). In a 100 mL double-jacket glass reactor equipped with magnetic stirring and a condenser, silicon tetrachloride (28 mL, 0.25 mol) was added dropwise to a solution of acetophenone (10.00 g, 0.083 mol) in absolute ethanol (60 mL) at 0 °C and a white precipitate was formed immediately. The reaction mixture was then refluxed for 12 h to ensure the complete formation of the product. After cooling to room temperature, the white product was filtered, washed with cold ethanol, recrystallized from isopropanol and dried at 120 °C for 3 h under vacuum. Yield 72%; ^{1}H NMR (300 MHz, DMSO-d$_6$): δ(ppm) 7.87 (s, 3H), 7.85 (d, 6H), 7.51 (dd, 6H), 7.40 (dd, 3H).

2.2. Synthesis of the Porous Polymers Networks (PPNs)

All the PPNs were synthesized in the same way, by combining triptycene and 1,3,5-TPB with isatin and TFAP. The reaction yields, in all cases, were higher than 95%. As an example, the preparation of the Triptycene-Isatin network is described below:

An oven-dried three-necked, 50 mL, Schlenk flask equipped with a mechanical stirrer and gas inlet and outlet was charged with triptycene (3.49 g, 13.8 mmol), isatin (3.06 g, 20.8 mmol) and chloroform (15 mL). The mixture was stirred at room temperature under a nitrogen blanket, cooled to 0 °C and trifluoromethanesulfonic acid (30 mL) was then slowly added with an addition funnel for 15-20 min. The reaction mixture was allowed to warm to room temperature and stirred for 5 days. The product was poured into a water/ethanol mixture (3/1), filtered and consecutively washed with water, acetone and chloroform. After drying at 150 °C for 12 h in vacuum, the material was obtained as a tan powder in 97.5 % yield.

2.3. Techniques

Fourier Transform Infrared (FT-IR) spectra were registered on a Perkin Elmer Spectrum RX-I FT-IR spectrometer, equipped with an ATR accessory. Solid state ^{13}C cross-polarization magic angle spinning NMR spectra (CP-MAS ^{13}C NMR) were recorded on a Bruker Avance 400 spectrometer equipped with a 89 mm wide bore and a 9.4 T superconducting magnet. The spectrometer operated at a Larmor frequency of 100 MHz using a contact time of 1 ms and a delay time of 3 s. All samples were spun at 9 KHz. Thermogravimetric analysis (TGA) was performed on a TA-Q500 analyzer under nitrogen flux (60 mL min^{-1}) at 10 °C min^{-1}. Wide-angle-X-ray scattering (WAXS) patterns were recorded in the reflection mode at room temperature, using a Bruker D8 Advance diffractometer provided with a Goebel Mirror and a PSD Vantec detector. CuKα (wavelength $\lambda = 1.54$ Å) radiation was used. A step-scanning mode was employed for the detector, with a 2θ step of 0.024° and 0.5 s per step. Scanning electron microscopy (SEM) images were taken with a QUANTA 200 FEG ESEM on Au-metallized samples operating at an acceleration voltage of 1.5 kV in high vacuum and using the detection of secondary electrons method.

Porous texture characterization of the polymers was carried out from their N_2 adsorption-desorption isotherms measured at –196 °C (77 K) in a volumetric device ASAP 2010 (Micromeritics) in the 10^{-6} – 0.995 relative pressures (P/P$_0$) range. The minimum equilibrium time (both for the adsorption and desorption) was 300 seconds. Samples were degassed at 125 °C for 18 h under vacuum, before the sorption measurements, to eliminate the sample humidity and any other adsorbed gases. The adsorption branch of the isotherms was used to obtain the apparent surface area (S$_{BET}$) by applying the Brunauer-Elmmett-Teller method in the 0.01 to 0.2 P/P$_0$ range, the micropore volume (V$_{micro}$) using the Dubinin-Radushkevich (DR) equation in the 0.001 to 0.2 range and the

total pore volume (V_{total}) as the volume of liquid nitrogen adsorbed at 0.975 relative pressure.

The CO_2 adsorption capacities of the polymers at 0 and 25 ºC (273 and 298 K) were measured in a volumetric device Nova 4200 (Quantachrome). Samples were also degassed at 125 ºC for 18 h under vacuum before the CO_2 adsorption measurements. From the CO_2 adsorption isotherms at 0 ºC, the narrow micropore volume (V_{nmicro}, pore width smaller than about 0.7 nm) was obtained by applying the DR equation in the 10^{-4} to 0.03 P/P_0 range. The cumulative pore volume and the pore size distributions were also obtained from the CO_2 isotherms at 0 ºC by the NL-DFT method.

N_2 and CO_2 adsorption-desorption isotherms up to 30 bar were measured gravimetrically at 25 ºC in a high pressures magnetic suspension balance (Rubotherm). The samples were degassed in situ in the balance, at 120 ºC under vacuum until constant weight. The buoyancy effects related to the gas displacement by the sample, sample holder, and other balance components were corrected by means of helium displacement.[45,46]


3. RESULTS AND DISCUSSION

### 3.1. Synthesis and characterization of PPNs

The synthesis of porous polymer networks was accomplished by treatment of triptycene or 1,3,5-triphenylbencene (1,3,5-TPB), which acted as trifunctional nucleophilic monomers, with isatin or 2,2,2-trifluoroacetophenone (TFAP), which acted as bifunctional electrophilic ones, in the presence of a mixture of trifluoromethanesulfonic acid and chloroform for 5 days at room temperature. Under superacidic conditions, the ketone derivatives containing electron-withdrawing groups were first activated through protonation, followed by electrophilic aromatic substitution on the aromatic system. The

combination of activated carbonyl compounds bearing electron-withdrawing groups and superacidic conditions permitted to assure a good reactivity and all of the PPNs were obtained with almost quantitative yields. To achieve the complete reaction, the proportion of trifunctional monomer to bifunctional one was kept at 2/3.

As expected, the obtained PPNs were insoluble in organic solvents and even in very low pK_a acids. Their chemical structures were characterized by ATR-FTIR (Figure 1) and CP/MAS ^{13}C NMR (Figure 2). The absorption bands at 1708, 1469, and 1320 cm^{-1} in the spectra of the isatin-based networks demonstrated the existence of 5-membered lactam rings coming from the isatin. The appearance of a broad band in the 3000-3600 cm^{-1} region was assigned to humidity traces in the samples, favored by the sorption of the amide groups (Figure S1 in the Supporting Information section). However, the presence of a small amount of tertiary alcohols, which were formed in the first stage of reaction (Scheme 1), could also be possible, if they have not undergone the ulterior protonation to provide the corresponding tetra-substituted methane derivatives. In the case of networks derived from TFAP, the absence of the carbonyl group band at about 1730 cm^{-1} and of the hydroxyl stretching bands above 3000 cm^{-1} confirmed the complete conversion of the ketone monomer. CP/MAS ^{13}C NMR spectra of Triptycene-Isatin and 1,3,5-TPB-TFAP are shown as examples in Figure 2. In all the systems, the peaks at 100-160 ppm were ascribed to carbon atoms in the aromatic rings and the peak at 62 ppm was assigned to the quaternary carbon at the ketone moiety, which was formed during the reaction. Additionally, other peaks at 180 and 55 ppm corresponding to the carbonyl groups of lactam rings and the methylidyne bridge carbons, respectively, were also seen.
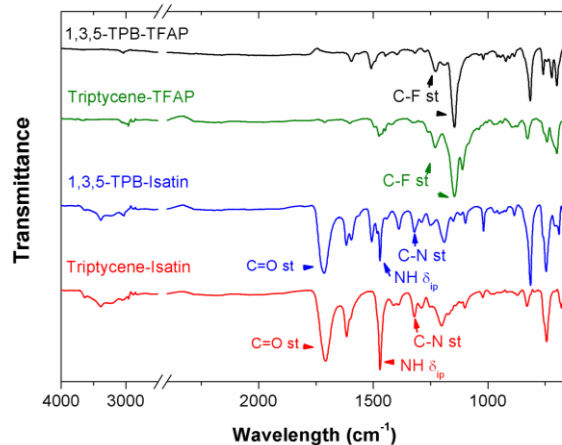
Figure 1. ATR-FTIR spectra of the PPNs.
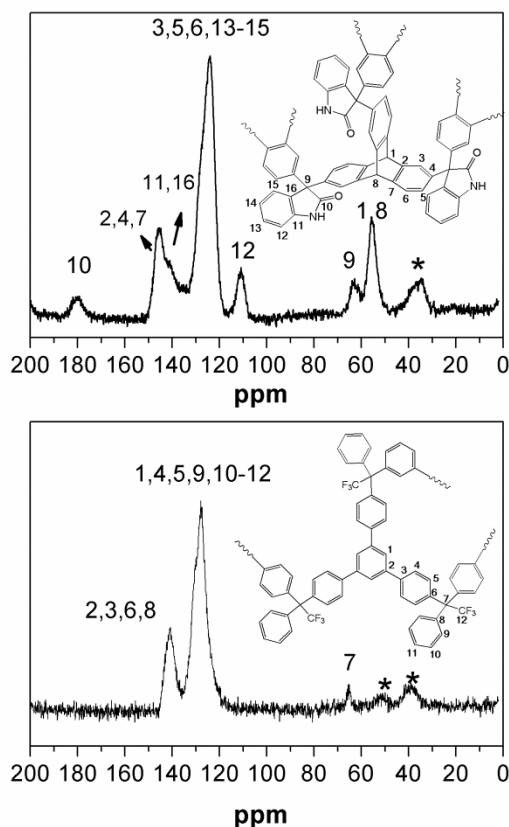
Figure 2. Solid state CP-MAS ^{13}C NMR spectra of Triptycene-Isatin (up) and 1,3,5-TPB-TFAP (bottom). Asterisks denote spinning side bands.

Wide-angle powder X-ray diffraction (Figure 3) confirmed that all networks were amorphous, although those containing 1,3,5-TPB showed some regularity in the chains packing, with at least two clear preferential intersegmental distances at 13.9° and 18.9°

(2θ), which correspond to 0.64 and 0.47 nm. This higher regularity in the packing was related to the planar-triangular shape of 1,3,5-TPB because it could favor the formation of π-π stacking into the network.
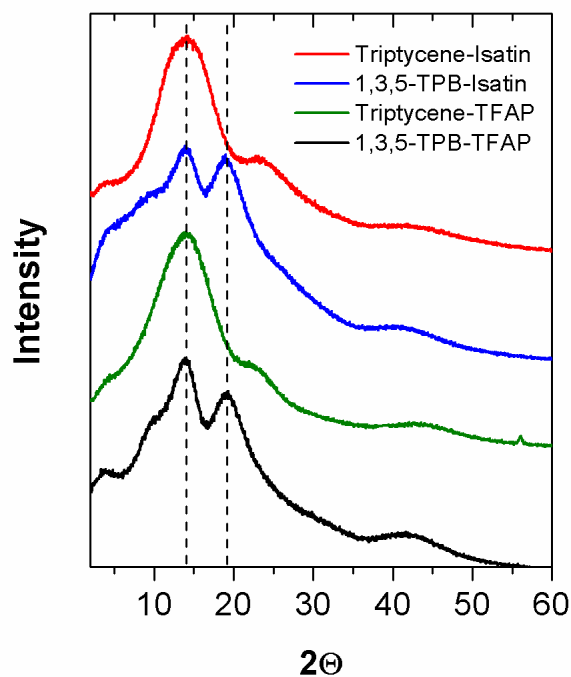
Figure 3. Wide-angle X-ray diffractograms of the PPNs.

The surface morphologies of the four PPNs were examined by FE-SEM (Figure 4). Triptycene-Isatin and Triptycene-TFAP networks consisted of loose agglomerates of tiny particles with rough surfaces and irregular shapes. 1,3,5-TPB-Isatin network was made up of spherical particles of very variable size. In contrast with the other PPNs, the images of 1,3,5-TPB-TFAP network revealed a homogeneous rough surface in which neither agglomerates nor particles were distinguished, probably due to the presence of very small size particles.
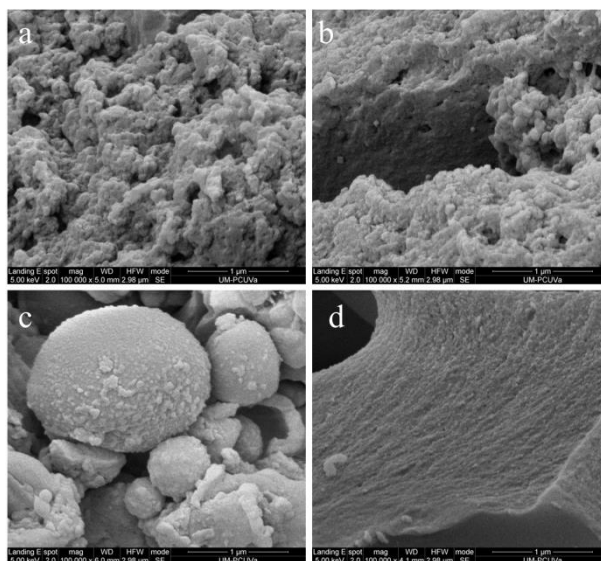
Figure 4. FE-SEM images of the PPNs: (a) Triptycene-Isatin, (b) 1,3,5-TPB-Isatin, (c) Triptycene-TFAP, and (d) 1,3,5-TPB-TFAP.

The resulting networks showed superb thermal stability both in nitrogen and in air atmosphere, as revealed by TGA (Figure 5). The degradation temperatures in both atmospheres and the char yield at 800 ºC in nitrogen are listed in Table 1. The char yields were very high, about 75% in all samples, as expected for highly aromatic systems having no hinges between the aromatic rings.

Table 1. Parameters of thermal stability of the PPNs.

PPN	$R_{800\,°C}$[a]	Degradation Temperature[b]	
		Nitrogen	Air
Triptycene-Isatin	75	520	425
1,3,5-TPB-Isatin	74	535	465
Triptycene-TFAP	74	490	430
1,3,5-TPB-TFAP	76	500	470

[a] char yield at 800 ºC (%) in nitrogen atmosphere. [b] Temperature (ºC) corresponding to a 2% mass loss.
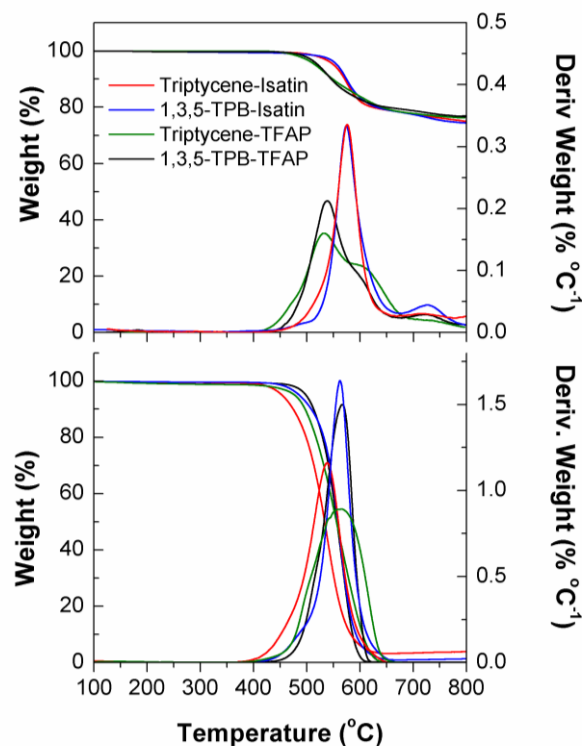
Figure 5. TGA thermograms of the PPNs in nitrogen (up) and in air (bottom) atmosphere.

3.2. Porosity characterization

The porosity of the PPNs was investigated by low-pressure sorption measurements using N_2 at -196 ºC. The adsorption/desorption isotherms of the samples are displayed in Figure 6. All the PPNs showed a sharp uptake at low relative pressures ($P/P_o < 0.01$) in the adsorption branch, implying a significant microporosity. However, unlike the microporous materials, which exhibit type I isotherms, according to IUPAC classification,[47] the adsorption branch did not reach a plateau when the relative pressure increased (typically between $0.2 \leq P/P_o \leq 0.8$) and the desorption branch showed a remarkable hysteresis down to low relative pressures. The slope between 0.2 and 0.8, and the volume difference between the adsorption and desorption branches was higher in the case of Triptycene-TFAP. As a result, the additional N_2 uptake at a relative pressure P/P_0 = 0.2 was 21% for networks prepared with isatin, 27% for 1,3,5-TPB-TFAP and 33% for Triptycene-TFAP. This behavior has already been reported for microporous networks, but

14

no detailed understanding has been achieved so far. The low-pressure hysteresis has been usually attributed to swelling phenomena or to restricted diffusional access in very narrow micropores. The first case is associated to a dual-mode sorption model, where the pores are first filled with gas molecules, and an additional Henry sorption, which is proportional to the pressure, occurs due to swelling (formation of new pores or growth in size of preexistent ones).[48] The second one is related to diffusional aspects (restricted filling of preexistent pores) due to the microporous morphology.[49] In this context, the possible causes of hysteresis in these PPNs will be discussed along the section.
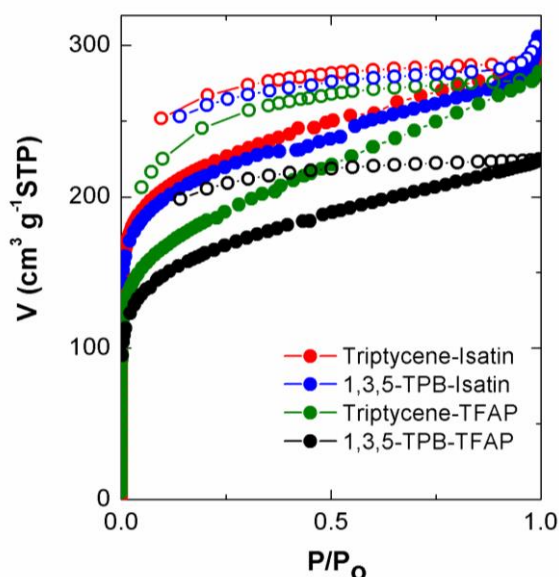
Figure 6. N_2 adsorption (full symbols)/desorption (empty symbols) isotherms measured at – 196°C for the PPNs.

Here we want to point out that the equilibration times for the N_2 isotherms were long enough to allow filling and emptying the micropores (pore width < 2 nm). To verify it, two isotherms were obtained varying the equilibrium time (300 or 1200 seconds) and fixing the minimum equilibration delay in each of the points at low relative pressures (P/P_0 < 0.2) as 1 and 10 hours. The effect of the equilibrium time on the amount of N_2 adsorbed for Triptycene-TFAP, the network with the highest hysteresis, is shown in Figure

15

7. The increase in the equilibrium setting allowed a slight rise in the amount of N_2 adsorbed at the lowest relative pressures ($P/P_o < 0.01$), confirming the existence of diffusional limitations caused by restricted-access pores. Above that relative pressure, however, both isotherms overlapped, within the experimental error, and reached the same N_2 uptake. Therefore, as no diffusional limitations can be detected when the pressure rises, the continuous increase of the slope is probably due to some swelling phenomena.
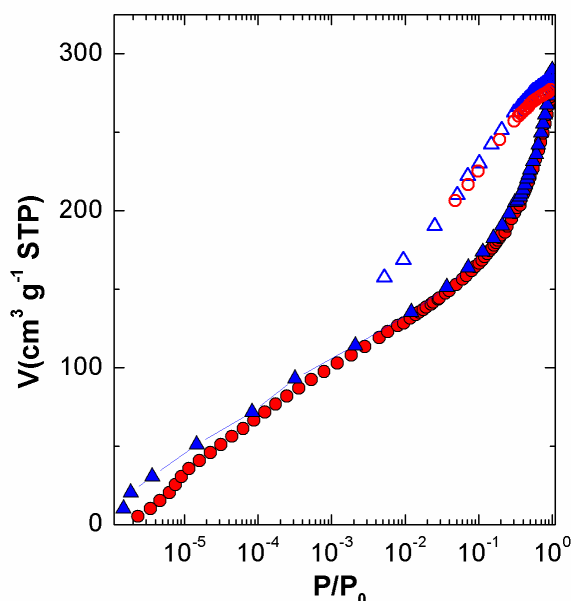
Figure 7. N_2 adsorption (full symbols)/desorption (empty symbols) isotherms for Triptycene-TFAP PPN at -196 ºC at different equilibrium time/minimum equilibration delay: 300 s/1 h (circles) and 1200 s/10 h (triangles).

In order to get insight into the microporosity of the samples, the CO_2 adsorption/desorption isotherms of the PPNs at 0 ºC and pressures up to 1 bar (Figure 8a) were also analyzed. The low-pressure CO_2 adsorption at this temperature has been demonstrated as a complementary method for the characterization of the narrow microporosity of different adsorbents.[50,51] The higher adsorption temperature, well above the CO_2 condensation temperature of -78 ºC, results in a larger kinetic energy, decreasing the diffusion limitations in the narrow micropores.
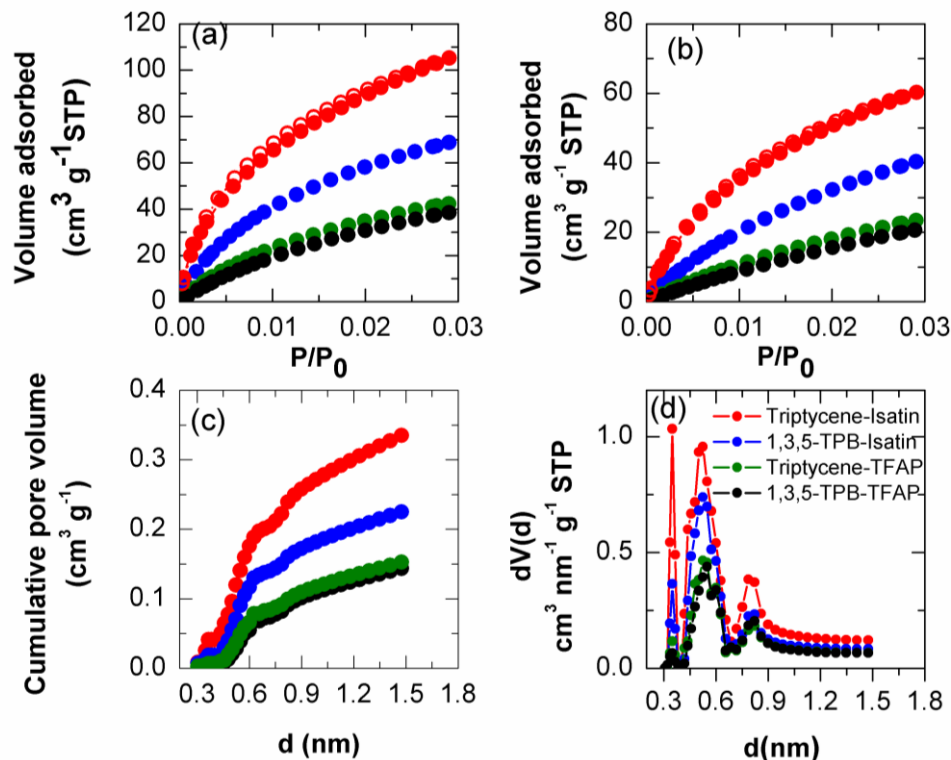
Figure 8. CO$_2$ adsorption (full symbols)/desorption (empty symbols) at 0 ºC (a) and 25 ºC (b) of PPNs, cumulative pore volume (c) and narrow micropore-size distribution (d) obtained by DFT from the CO$_2$ adsorption isotherms at 0 ºC.

The cumulative pore volume curves and the narrow micropore-size distribution, obtained by the method based on density functional theory (DFT), from the CO$_2$ adsorption isotherms at 0 ºC, are shown in Figure 8 (c and d). The pore size distributions of the four PPNs exhibited three peaks: the first one at pore sizes lower than 0.4 nm, the second one, of highest intensity, centered at 0.5 nm and the third one, of lowest intensity, at 0.8 nm. The minimum at 0.4 nm might be due to an artifact of the DFT method,[52] but, even if it were so considered, the networks presented a considerable contribution of narrow pores (smaller than 0.7 nm). As it can be seen in Figure 8c, Triptycene-Isatin has the highest volume of pores < 0.7 nm (0.20 cm^3 g^{-1}), followed by 1,3,5-TPB-Isatin (0.14 cm^3 g^{-1}), then by Triptycene-TFAP (0.08 cm^3 g^{-1}) and by 1,3,5-TPB-TFAP (0.07 cm^3 g^{-1}).

Therefore, the PPNs derived from isatin have the highest proportion of the narrowest micropores compared to those made from TFAP.

The porosity parameters obtained from N_2 and CO_2 adsorption at -196 and 0 °C, respectively, for all the PPNs, are summarized in Table 2.

Table 2. Porosity parameters of PPNs from N_2 and CO_2 adsorption isotherms.

PPN	N_2 adsorption isotherm			CO_2 adsorption	
	V_{total}[a]	S_{BET}[b]	V_{micro}[c]	V_{nmicro}[d]	$V_{micro}(HP)$[e]
	77 K, up to 1 bar			273 K	298 K
Triptycene-Isatin	0.44	790	0.31	0.36	0.38
1,3,5-TPB-Isatin	0.44	760	0.31	0.28	0.34
Triptycene-TFAP	0.43	655	0.25	0.19	0.24
1,3,5-TPB-TFAP	0.34	580	0.24	0.19	0.23

[a] total pore volume ($cm^3\ g^{-1}$) calculated from single point measurement at $P/Po = 0.975$.
[b] Surface area ($m^2\ g^{-1}$). [c] micropore volume ($cm^3\ g^{-1}$). [d] narrow micropore volume ($cm^3\ g^{-1}$) determined from low-pressure measurements (up to 1 bar). [e] micropore volume ($cm^3\ g^{-1}$) determined from high-pressure measurements (up to 30 bar).

The S_{BET} varied from 580 to 790 $m^2\ g^{-1}$ and the highest values corresponded to the isatin-based PPNs, which also had the highest values of micropore volume. Moreover, the ratio between the volumes of narrow micropores (V_{nmicro}) and micropores accessible to N_2 (V_{micro}) indicated that the micropore distribution seems to depend on the reacting ketone. Hence, for the case of isatin-based networks, in particular for Triptycene-Isatin PPN, there is a higher proportion of narrow micropores, many of them not accessible to the N_2 ($V_{nmicro} > V_{micro}$), while for the two TFAP-based ones, there is a significantly higher proportion of wider micropores ($V_{nmicro} < V_{micro}$).

The contribution of the narrow microporosity to the total pore volume (V_{total}) was estimated from V_{nmicro}, and the values are as follows: 82% for Triptycene-Isatin, 64% for 1,3,5-TPB-Isatin, 56% for 1,3,5-TPB-TFAP and 44% for Triptycene-TFAP, confirming the microporous character of these polymers. The lower values shown for the two PPNs derived from TFAP, and especially for Triptycene-TFAP, could be due to a higher swelling of the network. Regardless of this fact, the results shown so far seem to indicate that isatin favors the formation of narrow micropores and, moreover, its combination with triptycene yields highly microporous networks.

3.3. Low-pressures gas uptake of CO_2

The CO_2 adsorption/desorption isotherms were also measured at 25 ºC and 1 bar (Figure 8b). The values of CO_2 uptake at 0 and 25 ºC and 1 bar for all the PPNs, are listed in Table 3. The CO_2 uptakes at 0 ºC of the four PPNs showed the following order: Triptycene-Isatin had the highest value (207 mg g^{-1}/4.70 mmol g^{-1}), followed by 1,3,5-TPB-Isatin (135 mg g^{-1}/3.07 mmol g^{-1}), then by Triptycene-TFAP (83 mg g^{-1}/1.89 mmol g^{-1}) and finally by 1,3,5-TPB-TFAP (76 mg g^{-1}/1.72 mmol g^{-1}). As expected in a physisorption process, the adsorption capacity of CO_2 decreased when temperature increased and was between 41 and 45% lower at 25 ºC. It is noteworthy that the CO_2 adsorption at subatmospheric pressures was completely reversible for all the PPNs, indicating the possibility of regeneration of these materials by vacuum without applying heat.

Table 3. CO_2 and N_2 uptakes and isosteric heats of CO_2 adsorption for PPNs.

PPN	CO_2 at 1 bar[a]			CO_2 at 30 bar[b]	N_2 at 30
	273	298 K	Q_{st}	298 K	298 K
Triptycene-Isatin	207	118	35.3	407	52
1,3,5-TPB-Isatin	135	79	31.8	365	44

Triptycene-TFAP	83	46	29.6	252	34
1,3,5-TPB-TFAP	76	40	28.3	247	33

[a] Gas uptake (mg g^{-1}) and isosteric enthalpies of adsorption, Q_{st}, (kJ mol^{-1}). [b] Excess gas uptake (mg g^{-1}).

The CO_2 uptakes at 0 ºC of these PPNs can be compared with those of other networks containing triptycene or 1,3,5-TPB, such as azo-linked polymers (ALPs), (5.34-3.5 mmol g^{-1}),[53] triazole-linked polymers (TNPs), (4.5-1.6 mmol g^{-1}),[54] polybenzimidazole networks (TBIs), (3.2-2.7 mmol g^{-1}),[55] benzimidazole-linked polymers (BILPs) (5.3-2.9 mmol g^{-1}),[23] benzoxazole-linked polymers (BOLPs) (3.1-2.9 mmol g^{-1}),[25] benzothiazole-linked polymers (BTLPs) (4.3-3.2),[25] Porous aromatic frameworks (PAFs) (4.7-3.3),[19] triazine-based benzimidazole-linked polymers (TBILPs), (5.1-2.6 mmol g^{-1}),[24] star triptycene-based microporous polymers (STPs) (4.1-3.7),[56] and microporous polyimides (MPI), (3.8-2.3 mmol g^{-1}).[57] Figure 9 compares the CO_2 uptakes at 0 ºC and 1 bar of the PPNs studied here and those previously reported containing triptycene (circles) or 1,3,5-TPB (squares). The data are shown as a function of the total pore volumes, which were taken in the P/P_o range between 0.90 and 1 from the N_2 or Ar adsorption isotherms. The scatter of the data was large and the linear correlation coefficient was poor (r= 0.17), indicating that the total pore volume is not the only factor that determines the CO_2 uptake in these PPNs. The CO_2 uptake of Triptycene-Isatin (207 mg g^{-1}) was only about 10 % lower than the two best values of the PPNs here considered, which correspond to ALP1 (236 mg g^{-1})[53] and TBILP2 (228 mg g^{-1})[24], although the total pore volumes of these two PPNs were considerably higher (0.66 and 0.60 cm^3 g^{-1}, respectively). As far as we know, the CO_2 uptake of ALP1 represents one of the highest values for all known porous organic polymers reported to date. Moreover, the adsorption capacity of all the other networks here considered was lower than that of Triptycene-Isatin, even though many of them have a significantly higher V_{total}. It should also be remarked that all the networks with V_{total}

above 0.5 cm^3 g^{-1} and high CO_2 adsorption contain triptycene in their structure. This result is likely due to the rigid, fused-ring skeleton and three-fold symmetry structure of triptycene that provides a high internal molecular free volume and high surface area. As an example, the networks derived from STPs, which were obtained by a triptycene-triptycene coupling reaction from trihalotriptycenes, showed high BET surfaces (> 1300 m^2 g^{-1}) and high total volumes and CO_2 uptakes at 25 ºC and 1 bar, up to 4.0 mmol g^{-1}.[56] However, the microporosity ratio (defined as V_{micro}/V_{total}) was about 0.46 while it was 0.70 for Triptycene-Isatin PPN. Thus, the narrow microporosity would be a factor to consider in the high CO_2 adsorption capacity of Triptycene-Isatin.

Another factor to be considered is the binding affinity of these PPNs to CO_2.[58,59] The isosteric heats were determined by using the Clausius-Clapyeron equation (see Section 2 in the Supporting Information) from the data collected at 0 and 25 ºC. The Q_{st} values at zero coverage for the PPNs fell in a range between 28.3 and 35.3 kJ mol^{-1} (See Table 3). The highest values corresponded to the PPNs made from isatin, presumably due to the presence of lactam groups, which could interact favorably with CO_2 molecules, and so contribute significantly to the high CO_2 uptake.
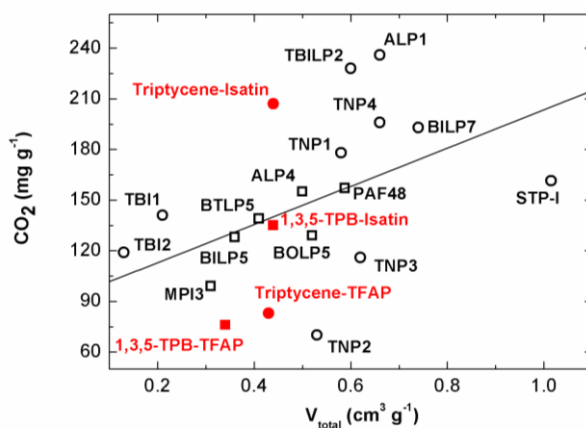
Figure 9. CO_2 uptake as a function of total pore volume for the PPNs and several porous organic polymers containing triptycene or 1,3,5-TPB in their structure.

To assess the effect of lactam groups and fluorine atoms (CF_3 moieties) on CO_2 binding interactions, we performed a DFT quantum mechanical study of the energy of interaction of two models (derived from the reactions of isatin and TFAP with benzene: Isatin-model and TFAP-model) in the presence of CO_2 (one and two molecules). All the details about the computational methods are provided in the Supporting Information section.

The electronic energy of the optimized geometries for both models and their CO_2-adducts are listed in Table S1. A favorable interaction of both models with CO_2 molecules was found. The binding affinity for the first CO_2 molecule was significantly higher for the Isatin-model than for the TFAP-model (20.741 vs 9.681 kJ mol^{-1}). However, the introduction of the second CO_2 molecule had roughly the same effect in the interaction energy for both models (around 11 kJ mol^{-1}). The binding affinity was also been estimated from the deviation of the OCO angle from the value of 180°, corresponding to the isolated CO_2. By comparing the values listed in the last column of Table S1, according to this criterion, the highest interaction corresponded to the Isatin-model-1CO_2 and to the first CO_2 of the Isatin-model-2CO_2. In TFAP-model the interaction with CO_2 was clearly lower in all cases, confirming the results obtained from the interaction energy.

Figure 10 shows the optimized geometry of the corresponding adducts with one and two molecules of CO_2. The interactions of the first CO_2 molecule with the Isatin-model (a) were through the O atom of the C=O in the lactam ring and the C atom in the CO_2 and through the N-H group and the O atom in the CO_2, with interatomic distances of 2.80 and 2.30 Å, respectively. For the TFAP-model (c), the C atom in the CO_2 molecule interacted with two F atoms of the CF_3 moiety (at distances of 2.97 and 3.07 Å). On the other hand, when two CO_2 molecules were allowed to interact with each model, a different orientation

of the CO_2 molecules was observed in each case, t-shape for Isatin-model (b) and crossed-shape for TFAP-model (d). In the Isatin-model, only one of the O atoms in the second CO_2 molecule interacts with the lactam ring, through the N-H. In the TFAP-model, the second CO_2 molecule interacted with the F atoms, in a way similar to the first one. Moreover, intermolecular interactions between both CO_2 molecules, $O=C=O(\delta-)\cdots C(\delta+)O_2$, were found, with bond distances of 2.95 and 3.25 Å for Isatin-model and TFAP-model, respectively. Consequently, this interaction should also favor the incorporation of successive CO_2 molecules.

These results support that the PPNs derived from isatin interact more favorably with CO_2 than those derived from TFAP, thus confirming the highest CO_2 uptake of these networks, even for similar values of V_{total}. However, considering that both the amount of lactam groups and the V_{total} are similar in the Triptycene-Isatin and 1,3,5-TPB-Isatin, the highest CO_2 adsorption for the first PPN is most likely due to the higher contribution of the narrow micropores to the total microporosity in that case.

Besides, taking into account that the Q_{st} values were comparable to or even superior to those found for ALPs [27.9-29.6 kJ mol^{-1}],[53] BILPs [26.7-28.8 kJ mol^{-1}],[23] TBILPs [29.0-35.6 kJ mol^{-1}][24] and TNPs [34.8-38.5 kJ mol^{-1}],[54] no correlation between the adsorption capacity and the isosteric heat of adsorption could be drawn from Figure 9. Thus, the total microporosity and pore size distribution seem to play a more relevant role in the CO_2 adsorption capacity of these organic porous networks at low pressures.
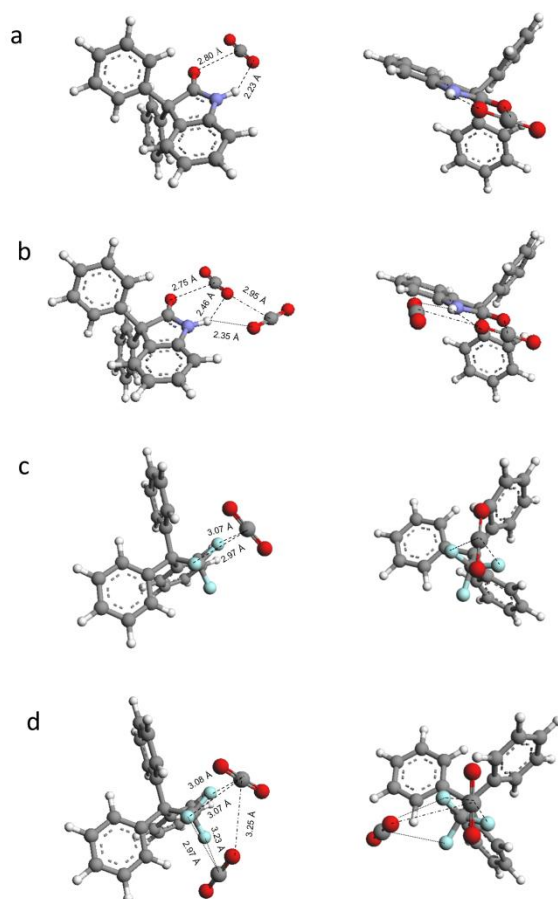
Figure 10. Optimized geometries for the CO_2-adducts (one and two CO_2 molecules) derived from Isatin-model (a and b) and TFAP-model (c and d). The lines are interatomic distances. The grey, white, red, blue and light-blue colors stand for C, H, O, N and F atoms, respectively.

3.4. High-pressures gas uptake of CO_2 and N_2

The high-pressure adsorption/desorption isotherms of the PPNs for N_2 and CO_2 at 25 ºC and up to 30 bar are displayed in Figure 11. For both gases, all the isotherms showed an increase in gas uptake with the increasing of gas pressure, without reaching a plateau, indicating that the pore volume filling was not complete over the pressure range considered. Despite the moderate S_{BET} values, these materials showed good CO_2 storage capacity, particularly those derived from isatin, as seen in Table 3. Triptycene-Isatin showed an excess CO_2 uptake of 40.7 wt.%, followed by 1,3,5-TPB-Isatin with a 36.5

wt.%, and then by the two TFAP-based PPNs with around 25 wt.% at 30 bar and 25 ºC. These values were between 3.5 and 6.2 times higher than those obtained at 1 bar and 25 ºC. It is remarkable that the PPNs derived of TFAP underwent the highest increase in adsorption capacity when the pressure increased from 1 to 30 bar. On its turn, the sorption of N_2 went from 5.2 wt.% for Triptycene-Isatin to 3.3 wt.% for the TFAP networks.

The high-pressure isotherms of N_2 for the PPNs were completely reversible without any hysteresis loop, which was expected because the measurements were conducted well above the gas condensation temperature. In the case of CO_2, the high-pressure isotherms were analogous to those obtained with N_2 at low pressures (up to 1 bar) and -196 ºC, because the relative pressure reached was 0.45 and some swelling can take place upon reaching these relative pressures. For CO_2, however, all of the trapped gas was easily released on returning to $P/P_o = 0$.

Moreover, the CO_2 adsorption experiments at high pressure permit a better determination of the total micropore volume of the PPNs by applying the DR equation, because the N_2 molecules cannot access to the narrowest micropores, as commented on above. However, the CO_2 molecules can be adsorbed in the whole microporosity range; if a high enough relative pressure is achieved. The volumes determined from CO_2 sorption at low-pressure/0 ºC and high-pressure/25 ºC, V_{nmicro} and $V_{micro}(HP)$, respectively (Table 2), were similar for Triptycene-Isatin, indicating that the pore size distribution was much narrower than for the other three PPNs and, moreover, it was mainly formed by pores having diameters lower than 0.7 nm. For the other three networks, the $V_{micro}(HP)$ was higher than V_{nmicro} showing that the pore size distribution was clearly wider and more heterogeneous. However, it is to be pointed out that the values of $V_{micro}(HP)$ were similar to those of V_{micro}, obtained from low-pressures N_2 isotherms, for the TFAP-based PPNs, indicating

that their microporosity was mainly due to pores with diameters higher than 0.45-0.50 nm.
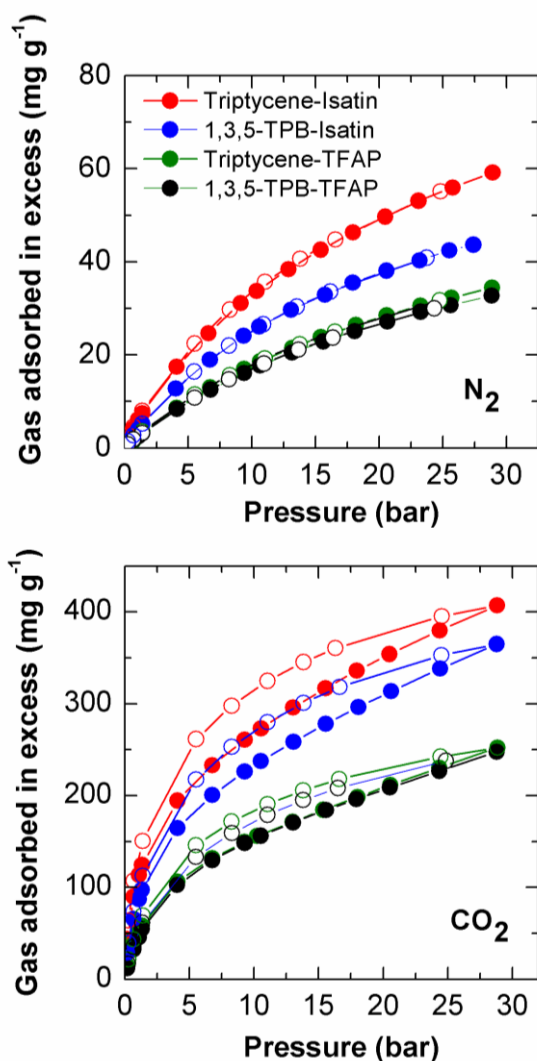
Figure 11. N_2 and CO_2 adsorption desorption isotherms of PPNs at 25 ºC up to 30 bar.

Another way of seeing that the microporosity size distribution is different in these PPNs is by comparing the characteristics curves of the adsorption measurements for CO_2 and N_2, which have been included in the Supporting Information (Section 4, Figure S4). In all cases, the overlapping of the CO_2 characteristic curves at low and high pressures was observed. However, the curves obtained from N_2 adsorption only overlapped with those corresponding to the high-pressure CO_2 adsorption at low values of $(A/\beta)^2$ (i.e. high P/P_0),

indicating the diffusional limitations of the N_2 to access at the narrowest pores, as commented on previously. This effect was notable in the case of Triptycene-Isatin, where a large deviation was observed even at very low values of $(A/\beta)^2$ (around 300 kJ^2 mol^{-2}), significantly lower than in the other PPNs, confirming its narrower porosity.

3.5. CO_2/N_2 Selectivity

Because these PPNs, and particularly those derived from isatin, showed high physicochemical stability and relatively good CO_2 storage capacity, we have studied their ability to selectively capture CO_2 over N_2. As commented on above, N_2 was much less adsorbed than CO_2, up to 30 bar and 25 ºC, which would be indicative of a good selectivity of CO_2 over N_2.

In a first attempt to evaluate the use of these PPNs as solid adsorbents in the capture of CO_2 from post-combustion flue gas,[60-63] the selectivity on a binary gas mixture (CO_2/N_2) was estimated by applying the SIPs adsorption model, which allows predicting the selectivity from single component isotherms. Detailed information about the calculations performed at high pressures and 25 ºC can be seen in the Supporting Information (Section 5). Figure 12 shows the CO_2/N_2 selectivity for binary mixtures with different CO_2 molar fraction (between 0.05 and 0.25) and pressure varying from 1 to 15 bar. The predicted selectivity for all the PPNs decreased when either the CO_2 mole fraction in the mixture or the pressure increased. The selectivity to separate CO_2/N_2 from a mixture with a composition similar to those of flue gases (15/85 %) and 1 bar pressure was 29.5 for Triptycene-Isatin, 32.7 for 1,3,5-TPB-Isatin, 28.6 for Triptycene-TFAP, and 22.5 for 1,3,5-TPB-TFAP.

In general, the performance in terms of CO_2 capacity and CO_2/N_2 selectivity were comparable, or even superior, to those of other microporous materials, such as porous

organic materials[23,53,54], carbon based materials,[64] and zeolitic imidazolate frameworks,[65] for similar flue gas composition and temperature and pressure conditions.
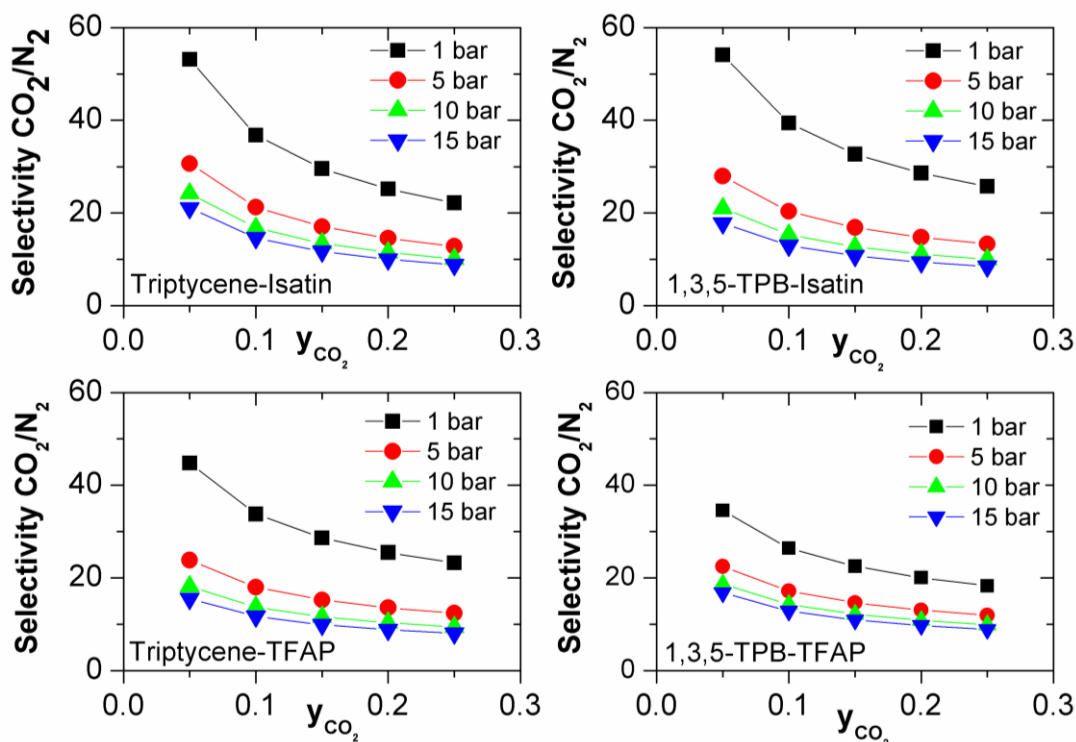
Figure 12. Selective adsorption of CO_2 over N_2 in a mixture of both gases at 25 ºC and different pressures as a function of the CO_2 mole fraction.

CONCLUSIONS

A new set of porous polymer networks (PPNs) from rigid trifunctional aromatic monomers and ketone derivatives were successfully prepared in quantitative yield using a cost-effective and feasible methodology, which is easily scaled up to produce large quantities of material for practical applications.

The PPNs were amorphous microporous materials with moderate surface areas (between 580 and 790 m^2 g^{-1}), good chemical stability and exceptional thermal resistance, even in air, with onset of degradation temperatures above 420 ºC.

The PPNs derived from isatin showed the highest CO_2 uptake together with the highest values of Q_{st}. This indicates a favorable chemical interaction between CO_2 and the lactam moieties, which has been confirmed by quantum mechanical calculations. However, if both PPNs from isatin are compared, the CO_2 uptake is significantly higher for the Triptycene-Isatin network. Therefore, the difference between both networks has to be attributed to their microporosity characteristics, because both have the same value of V_{total} and V_{micro} but Triptycene-Isatin PPN has a significantly higher contribution of narrow micropores to the total microporosity (82% of the total pore volume, versus 64%).

Because of the above, the CO_2 uptake for Triptycene-Isatin and the CO_2/N_2 selectivity under post-combustion capture conditions was comparable to those of the best PPNs reported up to now. The combination of these properties with the stability and synthetic feasibility commented on above, make them very promising as industrial CO_2 adsorbents.

SUPPORTING INFORMATION

Details on the calculations made from gas sorption measurements and on the quantum mechanical calculations. This material is available free of charge via the internet at http://pubs.acs.org.

AUTHOR INFORMATION

Corresponding Author

* E.mail: lozano@ictp.csic.es and cristina.alvarez@ictp.csic.es.

Author contributions

ORCID

Beatriz Lopez-Iglesias: 0000-0003-0198-1368

Fabián Suárez-García: 0000-0002-1970-293X

Carla Aguilar-Lugo: 0000-0003-4700-1564

Alfonso González Ortega: 0000-0002-9226-7807

Camino Bartolomé: 0000-0002-8492-6825

Jesús M. Martínez-Ilarduya: 0000-0003-4561-1131

José G. de la Campa: 0000-0003-1882-3104

Ángel E. Lozano: 0000-0003-4209-3842

Cristina Álvarez: 0000-0002-5000-0776

The research work was made through contributions of all authors.

The manuscript was written through contributions of Cristina Álvarez, José G. de la Campa, Ángel E. Lozano and Fabian Suárez-García.

REFERENCES

(1) Stocker, T.; Dahe, Q.; Plattner, G. -K.; Tignor, M.; Midgley, P. IPCC Expert Meeting on Assessing and Combining Multi Model Climate Projections. Meeting Report. National Center for Atmospheric Research: Boulder, Colorado, USA, 2010.

(2) Cao, L.; Caldeira, K. Atmospheric Carbon Dioxide Removal: Long-Term Consequences and Commitment. *Environ. Res. Lett.* **2010**, *5*, 24011-24016.

(3) Bodansky, D. The Durban Platform Negotiations: Goals and Options. Harvard Project on climate Agreements Viewpoint 2012. https://ssrn.com/abstract=2102994.

(4) Weber, E. U. Experience-Based and Description-Based Perceptions of Long-Term Risk: Why Global Warming Does Not Scare Us (Yet). *Climatic Change* **2006**, *77*, 103-120.

(5) Paterson, N. R. Global Warming: a Critique of the Anthropogenic Model and its Consequences. *Geosci. Can.* **2011**, *38*, 41–48.

(6) Kim, K. S. Public Understanding of the Politics of Global Warming in the News Media: the Hostile Media Approach. *Public Underst. Sci.* **2011**, *20*, 690–705.

(7) Haszeldine, R. S. Carbon Capture and Storage? How Green can Black Be. *Science* **2009**, *325*, 1647-1652.

(8) Sneddon, G.; Greenaway, A.; Yiu, H. H. P. The Potential Applications of Nanoporous Materials for the Adsorption, Separation, and Catalytic Conversion of Carbon Dioxide. *Adv. Energy Mater.* **2014**, *4*, 1301873-1301891.

(9) Dawson, R.; Cooper, A. I.; Adams, D. J. Nanoporous Organic Polymer Networks. *Prog. Polym. Sci.* **2012**, *37*, 530–563.

(10) McKeow, N. B.; Budd, P. M. Exploitation of Intrinsic Microporosity in Polymer-Based Materials. *Macromolecules* **2010**, *43*, 5163-5176.

(11) Das, S.; Heasman, P.; Ben, T; Qiu, S. Porous Organic Materials: Strategic Design and Structure−Function Correlation. *Chem. Rev.* **2017**, *117*, 1515-1563.

(12) Zhu, G.; Ren, H. *Porous Organic Frameworks*; Springer, Berlin, Heidelberg, 2015.

(13) Saleh, M.; Lee, H. M.; Kemp, K. C.; Kim, K. S. Highly Stable CO_2/N_2 and CO_2/CH_4 Selectivity in Hyper-Cross-Linked Heterocyclic Porous Polymers. *ACS Appl. Mater. Interfaces* **2014**, *6*, 7325–7333.

(14) Puthiaraj, P.; Ahn, W. S. CO_2 Capture by Porous Hyper-Cross-Linked Aromatic Polymers Synthesized Using Tetrahedral Precursors. *Ind. Eng. Chem. Res.* **2016**, *55*, 7917–7923.

(15) Dawson, R.; Stöckel, E.; Holst, J. R.; Adams, D. J.; Cooper A. I. Microporous Organic Polymers for Carbon Dioxide Capture. *Energy Environ. Sci.* **2011**, *4*, 4239-4245.

(16) Ben, T.; Pei, C.; Zhang, D.; Xu, J.; Deng, F.; Jing, X.; Qiu, S. Gas Storage in Porous Aromatic Frameworks (PAFs). *Energy Environ. Sci.* **2011**, *4*, 3991-3999.

(17) Ben, T.; Ren, H.; Ma, S.; Cao, D.; Lan, J.; Jing, X.; Wang, W.; Xu, J.; Deng, F.; Simmons, J. M.; Qiu, S.; Zhu. G. Targeted Synthesis of a Porous Aromatic Framework with High Stability and Exceptionally High Surface Area. *Angew. Chem. Int. Ed.* **2009**, *48*, 9457-9460.

(18) Chen, L.; Honsho, Y.; Seki, S.; Jiang, D. Light-Harvesting Conjugated Microporous Polymers: Rapid and Highly Efficient Flow of Light Energy with a Porous Polyphenylene Framework as Antenna. *J. Am. Chem. Soc.* **2010**, *132*, 6742–6748.

(19) Li, L.; Cai, K.; Wang, P.; Ren, H.; Zhu, G. Construction of Sole Benzene Ring Porous Aromatic Frameworks and Their High Adsorption Properties. *ACS Appl.Mater.Interfaces* **2015**, *7*, 201-208.

(20) Lu, W.; Yuan, D.; Zhao, D.; Schilling, C. I.; Plietzsch, O.; Muller, T.; Bräse, S.; Guenther, J.; Blümel, J.; Krishna, R.; Li, Z.; Zhou, H. -C. Porous Polymer Networks: Synthesis, Porosity, and Applications in Gas Storage/Separation. *Chem. Mater.* **2010**, *22*, 5964–5972.

(21) Lu, W.; Sculley, J. P; Yuan, D.; Krishna, R.; Wei, Z.; Zhou, H.-C. Polyamine-Tethered Porous Polymer Networks for Carbon Dioxide Capture from Flue Gas. *Angew. Chem. Int. Ed.* **2012**, *51*, 7480 –7484.

(22) Katsoulidis, A. P.; Kanatzidis, M. G. Phloroglucinol Based Microporous Polymeric Organic Frameworks with –OH Functional Groups and High CO_2 Capture Capacity. *Chem. Mater.* **2011**, *23*, 1818-1824.

(23) Rabbani G. M.; El-Kaderi, H. M. Synthesis and Characterization of Porous Benzimidazole-Linked Polymers and Their Performance in Small Gas Storage and Selective Uptake. *Chem. Mater.* **2012**, *24*, 1511−1517.

(24) Sekizkardes, A. K.; Altarawneh, S.; Kahveci, Z.; İslamoğlu, T.; El-Kaderi, H. M. Highly Selective CO_2 Capture by Triazine-Based Benzimidazole-Linked Polymers. *Macromolecules* **2014**, *47*, 8328−8334.

(25) Rabbani, M. G.; Islamoglu, T.; El-Kaderi, H. M. Benzothiazole- and Benzoxazole-Linked Porous Polymers for Carbon Dioxide Storage and Separation. *J. Mater. Chem. A* **2017**, *5*, 258-265.

(26) Zhu, Y.; Long, H.; Zhang, W. Imine-Linked Porous Polymer Frameworks with High Small Gases (H_2, CO_2, CH_4, C_2H_2) Uptake and CO_2/N_2. *Chem. Mater.***2013**, *25*, 1630-1635.

(27) Kuhn, P.; Antonietti, M.; Thomas, A. Porous, Covalent Triazine-Based Frameworks Prepared by Ionothermal Synthesis. *Angew. Chem. Int. Ed.* **2008**, *47*, 3450 –3453.

(28) Wang, K.; Huang, H.; Liu, D.; Wang, C.; Li, J.; Zhong, C. Covalent Triazine-Based Frameworks with Ultramicropores and High Nitrogen Contents for Highly Selective CO_2 Capture. *Environ. Sci. Technol.* **2016**, *50*, 4869−4876.

(29) Ren, S.; Bojdys , M. J.; Dawson, R.; Laybourn, A.; Khimyak, Y. Z.; Adams, D. J.; Cooper, A. I. Porous, Fluorescent, Covalent Triazine-Based Frameworks via Room-Temperature and Microwave-Assisted Synthesis. *Adv. Mater.* **2012**, *24*, 2357-2361.

(30) Ghanem, B. S.; Msayib, D. J.; McKeown, N. B.; Harris, K. D. M.; Pan, Z.; Budd, P. M.; Butler, A.; Selbie, J.; Book, D.; Walton, A. A Triptycene-Based Polymer of Intrinsic Microporosity that Displays Enhanced Surface Area and Hydrogen Adsorption. *Chem. Commun.* **2007**, *0*, 67-69.

(31) Grzybowski, M.; Skonieczny, K.; Butenschön, H.; Gryko, D. T. Comparison of Oxidative Aromatic Coupling and the Scholl Reaction. *Angew. Chem. Int. Ed.* **2013**, *52*, 9900–9930.

(32) Li, L.; Ren, H.; Yuan, Y.; Yu, G.; Zhu, G. Construction and Adsorption Properties of Porous Aromatic Frameworks via $AlCl_3$-Triggered Coupling Polymerization. *J. Mater. Chem. A.* **2014**, *2*, 11091-11098.

(33) Msayib, K. J.; McKeown, N. B. Inexpensive Polyphenylene Network Polymers with Enhanced Microporosity. *J. Mater. Chem. A.* **2016**, *4*, 10110–10113.

(34) Surya Prakash, G. K.; Panja, C.; Shakhmin, A.; Shah, E.; Mathew, T.; Olah, G. A. BF_3-H_2O Catalyzed Hydroxyalkylation of Aromatics with Aromatic Aldehydes and Dicarboxaldehydes: Efficient Synthesis of Triarylmethanes, Diarylmethyl benzaldehydes, and Anthracene Derivatives. *J. Org. Chem.* **2009**, *74*, 8659–8668.

(35) Preis, E.; Widling, C.; Scherf, U.; Patil, S.; Brunklaus, G.; Schmidt, J.; Thomas, A. Aromatic, Microporous Polymer Networks with High Surface Area Generated in Friedel–Crafts-Type Polycondensations. *Polym. Chem.* **2011**, *2*, 2186-2189.

(36) Olah, G. A. Superelectrophiles. *Angew. Chem. Int. Ed.* **1993**, *32*, 767-788.

(37) Klumpp, D. A. Superelectrophiles: Charge-Charge Repulsive Effects. *Chem. Eur. J.* **2008**, *14*, 2004-2015.

(38) O'Connor, M. J.; Boblak, K. N.; Topinka, M. J.; Kindelin, P. J.; Briski, J. M.; Zheng, C.;. Klumpp, D. A. Superelectrophiles and the Effects of Trifluoromethyl Substituents. *J. Am. Chem. Soc.* **2010**, *132*, 3266–3267.

(39) Kray, W. D.; Rosser, R. W. Synthesis of Multifunctional Triarylfluoroethanes. 1. Condensation of Fluoro Ketones. *J. Org. Chem.* **1977**, *42*, 1186–1189.

(40) Colquhoun, H. M.; Zolotukhin, M. G.; Khalilov, L. M.; Dzhemilev, U. M. Superelectrophiles in Aromatic Polymer Chemistry. *Macromolecules* **2001**, *34*, 1122–1124.

(41) Zolotukhin, M. G.; Fomina, L.; Salcedo, R.; Sansores, L.E.; Colquhoun, H. M.; Khalilov, L. M. Superelectrophiles in Polymer Chemistry. A Novel, One-Pot Synthesis of High-Tg, High-Temperature Polymers. *Macromolecules* **2004**, *37*, 5140–5141.

(42) Zolotukhin, M. G.; Fomine, S.; Lazo, L. M.; Salcedo, R.; Sansores, L. E.; Cedillo, G. G.; Colquhoun, H. M.; Fernandez-G, J. M.; Khalizov, A. F. Superacid-Catalyzed Polycondensation of Acenaphthenequinone with Aromatic Hydrocarbons. *Macromolecules* **2005**, *38*, 6005–6014.

(43) Nieto, D. R.; Zolotukhin, M. G.; Fomina, L.; Fomine, S. Superacid Mediated Hydroxyalkylation Reaction of 1,2,3-Indanetrione: a Theoretical Study. *J. Phys. Org. Chem.* **2010**, *23*, 878–884.

(44) Pulido, B. A.; Waldron, C.; Zolotukhin, M. G.; Nunes, S. P. Porous Polymeric Membranes with Thermal and Solvent Resistance. *J. Memb. Sci.* **2017**, *539*, 187–196.

(45) Sircar, S. Measurement of Gibbsian Surface Excess. AlChE J. **2001**, *47*, 1169-1176.

(46) Suárez-Ruiz, I.; Juliao, T.; Suárez-García, F.; Marquez, R.; Ruiz, B. Porosity Development and the Influence of Pore Size on the CH_4 Adsorption Capacity of a Shale Oil Reservoir (Upper Cretaceous) from Colombia. Role of Solid Bitumen. *Int. J. Coal Geol.* **2016**, *159*, 1–17.

(47) Thommes, M.; Kaneko, K.; Neimark, A. V.; Olivier, J. P.; Rodriguez-Reinoso, F.; Rouquerol, J.; Sing, K. S. W. Physisorption of Gases, with Special Reference to the Evaluation of Surface Area and Pore Size Distribution (IUPAC Technical Report). *Pure Appl. Chem.* **2015**, *87*, 1051–1069.

(48) Weber, J.; Antonietti, M.; Thomas, A. Microporous Networks of High-Performance Polymers: Elastic Deformations and Gas Sorption Properties. *Macromolecules* **2008**, *41*, 2880-2885.

(49) Jeromenok, J.; Weber, J. Restricted Access: On the Nature of Adsorption/Desorption Hysteresis in Amorphous, Microporous Polymeric Materials. *Langmuir* **2013**, *29*, 12982–12989.

(50) Lozano-Castelló, D.; Cazorla-Amorós, D.; Linares-Solano, A. Usefulness of CO_2 Adsorption at 273 K for the Characterization of Porous Carbons. *Carbon* **2004**, *42*, 1233–1242.

(51) Rouquerol, F.; Rouquerol, J.; Sing, K. S. W. Adsorption by Powders & Porous Solids. Principles, Methodology and Applications, Academic Press, New York, 1999.

(52) Jagiello, J.; Thommes, M. Comparison of DFT Characterization Methods Based on N_2, Ar, CO_2, and H_2 Adsorption Applied to Carbons with Various Pore Size Distributions. *Carbon* **2004**, *42*, 1225–1229.

(53) Arab, P.; Rabbani, M. G.; Sekizkardes, A. K.; İslamoğlu, T.; El-Kaderi, H. M. Copper (I)-Catalyzed Synthesis of Nanoporous Azo-Linked Polymers: Impact of Textural Properties on Gas Storage and Selective Carbon Dioxide Capture. *Chem. Mater.* **2014**, *26*, 1385−1392.

(54) Mondal, S.; Das, N. Triptycene based 1,2,3-Triazole Linked Network Polymers (TNPs): Small Gas Storage and Selective CO_2 Capture. *J. Mater. Chem. A*. **2015**, *3*, 23577-23586.

(55) Zhao, Y-C.; Cheng, Q.-Y.; Zhou, D.; Wang, T.; Han, B-H. Preparation and Characterization of Triptycene-Based Microporous Poly(Benzimidazole) Networks. *J. Mater. Chem.* **2012**, 22, 11509-11514.

(56) Zhang, C.; Liu, Y.; Li, B.; Tan, B.; Chen, C. -F.; Xu, H. –B.; Yang, X. –L. Triptycene-Based Microporous Polymers: Synthesis and their Gas Storage Properties. *ACS Macro Lett.* **2012**, *1*, 190-193.

(57) Li, G.; Wang, Z. Microporous Polyimides with Uniform Pores for Adsorption and Separation of CO_2 Gas and Organic Vapors. *Macromolecules* **2013**, *46*, 3058-3066.

(58) Islamoglu, T.; Behera, S.; Kahveci, Z.; Tessema, T. –D.; Jena, P.; El-Kaderi, H. M. Enhanced Carbon Dioxide Capture from Landfill Gas Using Bifunctionalized Benziimidazole-Linked Polymers. *ACS Appl. Mater. Interfaces* **2016**, *8*, 14648-14655.

(59) Thirion, D.; Rozyyev, V.; Park, J.; Byun, J.; Jung, Y.; Atilhan, M.; Yavuz, D. T. Observation of the Wrapping Mechanism in Amine Carbon Dioxide Molecular Interactions on Heterogeneous Sorbents. *Phys. Chem. Chem. Phys.* **2016**, *18*, 14177-14181.

(60) Boot-Handford, M. E.; Abanades, J. C.; Anthony, E. J.; Blunt, M. J.; Brandani, S.; Dowell, N. M.; Fernández, J. R.; Ferrari, M-C.; Gross, R.; Hallett, J. P.; Haszeldine, R. S.; Heptonstall, P.; Lyngfelt, A.; Zen Makuch, Z.; Mangano, E.; Richard T. J. Porter, R. T. J.; Pourkashanian, M.; Rochelle, G. T.; Shah, N.; Joseph G. Yao, J. Y.; Paul S. Fennell, P. S. Carbon Capture and Storage Update. Energy Environ. Sci. **2014**, *7*, 130-189.

(61) Wang, Q.A.; Luo, J. Z.; Zhong, Z. Y.; Borgna, A. CO_2 Capture by Solid Adsorbents and their Applications: Current Status and New Trends. Energy Environ. Sci. **2011**, *4*, 42-55.

(62) Olajire, A. A. CO_2 Capture and Separation Technologies for End- of-Pipe Applications – a Review. *Energy* **2010**, *35*, 2610–28.

(63) Espinal, L.; Poster, D. L.; Wong-Ng, W.; Allen, A. J.; Green, M. L. Measurement, Standards, and Data Needs for CO_2 Capture Materials: A Critical Review. *Environ. Sci. Technol.* **2013**, *47*, 11960-11975.

(64) Radosz, M.; Hu, X.; Krutkramelis, K.; Shen, Y.; Flue-Gas Carbon Capture on Carbonaceous Sorbents: Towards a Low-Cost Multifunctional Carbon Filter for "Green" Energy Producers. *Ind. Eng. Chem. Res.***2008**, *47*, 3783-3794.

(65) Banerjee, R.; Furukawa, H.; Britt, D.; Knobler, C.; O'Keeffe, M.; Yaghi, O. M. Control of Pore Size and Functionality in Isoreticular Zeolitic Imidazolate Frameworks and their Carbon Dioxide Selectivity Capture Properties.